Chemical Engineering Journal 481 (2024) 148655

Contents lists available at ScienceDirect

Chemical Engineering Journal

journal homepage: www.elsevier.com/locate/cej

Efficient electro-demulsification of O/W emulsions and simultaneous oil removal enabled by a multiscale porous biocarbon electrode

Kui Wang [a,b], Hailiang Zhao [c], Yingming Zhang [c], Xu Li [a], Mengyi Xu [a], Meirong Song [a], Guangxin Ru [g], Xiaolei Jiang [a], Xiuhong Zhu [g], Dandan Han [a], Yutao Dong [a], Kexin Shen [a], Xinchang Pang [e], Yuanyuan Li [d,*], Yixiang Zhang [b,*], Xia Sheng [a,b,d,e,f,*]

[a] College of Sciences, Henan Agricultural University, Nongye Road 63, 450002 Zhengzhou, China
[b] Zhengzhou Public Utilities Investment Development Co., LTD, Shang Ding Road 89, 450016 Zhengzhou, China
[c] School of Environmental Engineering, Henan University of Technology, Lianhua Street 100, 450001 Zhengzhou, China
[d] Department of Fibre and Polymer Technology, Wallenberg Wood Science Center, KTH Royal Institute of Technology, Stockholm 10044, Sweden
[e] Materials Science and Engineering, Zhengzhou University, Science Avenue 100, 450001 Zhengzhou, China
[f] Huaxia Green Water Technology Co., LTD, Dongfeng South Road 36, 450046 Zhengzhou, China
[g] College of Forestry, Henan Agricultural University, Nongye Road 63, Zhengzhou 450002, China

ARTICLE INFO

Keywords:
Electro-demulsification
Low voltage
Low energy consumption
Biomass
Multiscale pores structure
Carbonized birch

ABSTRACT

Emulsion wastewater contain substantial amounts of oil and various additives, which pose threats to the environment and human health. Demulsification is a crucial pretreatment stage for wastewater. This study aims to identify a novel electro-demulsification method with high oil removal efficiency and low energy consumption. Modified carbonized birch wood with a unique isotropic multiscale pore structure is used as a self-standing electrode to treat a toluene oil-in-water (O/W) emulsion. The electrode must have a highly porous structure to facilitate efficient water diffusion and oil adsorption. It must also have high electronic conductivity to expedite polarized molecular electrophoresis to realize penetration into the pores and, subsequently, demulsification. Guided by an applied electric field force, polarized O/W droplets are drawn toward the electrode, revealing electrical characteristics distinct from those of polarized organic molecules. This electric field force augments the capture and adhesion of droplets by the electric double layer at the electrode interface. Consequently, adsorbed droplets in close proximity to the electrode rupture due to the combined influence of the electric field force and the electrostatic effects stemming from the electrode's multiscale porous structure. This synergistic action enables demulsification to occur efficiently at low energy consumption levels. This study has revealed that electro-demulsification can effectively treat toluene emulsions stabilized by various surfactants and microemulsion containing toluene. Therefore, this electro-demulsification technology can be further developed for various types of water pollution.

1. Introduction

Various industrial processes, including those applied in the metal processing, pharmaceutical, cosmetics, food, and crude oil industries, produce a substantial quantity of oil-containing emulsified wastewater [1]. Oil-in-water (O/W) emulsified wastewater is prevalent, primarily comprising mineral oil, synthetic oil, water, and different additives [2], and often exhibiting complex compositions that are difficult to biochemically treat [3,4]. In industrial production, the presence of emulsions often leads to equipment wear, corrosion, and rust, consequently increasing operational and production expenses [5,6]. Oils, surfactants, and other additives in emulsions can be mutagenic and carcinogenic to human health, and they inhibit plant growth [7,8]. Many workers suffer from various skin diseases when exposed to cutting fluids [9,10].

The key problem in treating oily wastewater is breaking the emulsion [4]. Traditional demulsification methods can generally be categorized into several categories, such as chemical treatment, which can result in secondary pollution [11,12]. Although effective, biological treatment has limitations, such as a slow degradation speed and harsh reaction conditions [13]. Physical adsorption is another method, but it is

* Corresponding authors at: College of Sciences, Henan Agricultural University, Nongye Road 63, 450002 Zhengzhou, China (X. Sheng).
E-mail addresses: yua@kth.se (Y. Li), zhangyixiang@zzgyjt.cn (Y. Zhang), shengxia@henau.edu.cn (X. Sheng).

https://doi.org/10.1016/j.cej.2024.148655
Received 4 August 2023; Received in revised form 29 December 2023; Accepted 7 January 2024
Available online 11 January 2024

restricted by limited adsorption capacities and the separation process [14,15]. Although these treatment methods are relatively mature, they have drawbacks, which limit their applicability to simultaneous demulsification and oil remove [1]. Therefore, there is an urgent need to establish a novel demulsification method characterized by high efficiency, low energy consumption, cost-effectiveness, and no secondary pollution. Electro-demulsification offers several advantages, including environmental friendliness, cleanliness, simplicity, and high efficiency [16]. However, the high energy consumption increases the cost, and high-risk factors limit industrial application [18]. In previous studies, traditional demulsification methods using high direct current (DC) voltages at the kilovolt (kV) level have been used for water-in-oil (W/O) emulsions. For example, Woo-Taeg Kwon et al. [17] used voltages ranging from 2 to 5 kV to treat W/O emulsions but achieved a separation efficiency of less than 80 %. Tsuneki Ichikawa et al. [18,19] discovered that rapid demulsification of heavy oil O/W emulsions is possible with cationic connections. However, they reported a voltage reduction until 30 V.

Therefore, there is no precedent for treating emulsions using electro-demulsification combined with adsorption while realizing dramatically reduced energy consumption and improved removal efficiency. Consequently, we here describe, for the first time, the use of self-standing electrodes made from biomass-based carbon materials to treat oily emulsions through electro-demulsification. Wood possesses open channels along its growth direction that transport water, ions, and nutrients from the plant's roots to the rest of the plant. These channels form a distinctive anisotropic structure consisting of both mesopores and micropores [20–23], and this porous structure is responsible for the high specific surface area of biochar. Carbonized biomass carbon offers the advantages of excellent electrical conductivity, widespread availability, large-scale production, and cost-effectiveness [24,25].

In the demulsification experiments in this paper, electrodes operated without an applied voltage serve as controls to emphasize the impact of electro-demulsification. Drawing on the results of experiments, characterizations, modeling, and density functional theory (DFT) calculations, the mechanisms of electro-demulsification leading to demulsification and toluene removal are investigated systematically and comprehensively. The effects of voltage magnitude, toluene concentration, and surfactant type on the demulsification process and the electrode demulsification cycle are studied. This combined technology using multiscale self-standing carbonized birch electrodes may become popular for application in the treatment of different wastewaters.

2. Materials and methods

2.1. Methods for the preparation and characterization of electrodes

Birch electrodes were made via hydrothermal modification and carbonization. Initially, soaked birch was cut into a sheet of 5.0 × 0.3 × 1.5 cm^3. Soaking softens the wood, making it easier to cut it into the desired shapes without damaging its structure. The electrode-synthesized method was employed in our published work [26]. A total of 10.00 g of D-glucosamine hydrochloride (GlcN) (Biotech, Macklin, China) was dissolved in 100 mL of ultrapure water to obtain GlcN solution. A total of 1.00 g of $Fe_2(SO_4)_3{\cdot}7H_2O$ (AR, SCR, China) and 1.16 g of $NiCl{\cdot}6H_2O$ (AR, SCR, China) were dissolved in 100 mL of GlcN solution, resulting in an aqueous solution. The wood slice was impregnated with the mixture by vertically placing the wood in the solution. After ultrasonication (0.5 h), the hydrothermal reaction was performed in a Teflon-lined stainless-steel autoclave at 180 °C for 15.0 h [26]. Metal precursors (Ni^{2+} and Fe^{3+}) and GlcN were attached to the surfaces and pores of the wood. GlcN and hydroxyl groups in wood can fix metal cations and contribute to the formation of nanoparticles (NPs) in wood [27]. After the hydrothermal reaction, the surface of the birch was rinsed with acetone and ultrapure water to remove impurities. Then, the birch wood was completely submerged in a triangular flask containing a solution of acetone with 12.50 g/L 2,3-dihydroxynaphthalene (98 %, Macklin, China) under vacuum conditions for 12.0 h to remove organic impurities in the wood and to keep the pores open [26]. 2,3-Dihydroxynaphthalene can increase the degree of graphitization in the carbonization of biomass electrodes, leading to enhanced electrical conductivity. It also facilitates the formation of nitrogen-containing functional groups, improving the pore structure and surface area of the electrode material [28,29]. The hydrothermally modified wood was freeze-dried (Bilang, China) at −50 °C for 12.0 h to remove excess moisture and residual organic matter. Subsequently, the freeze-dried wood was toughened for carbonization treatment. Finally, under a N_2 protective atmosphere, the wood was carbonized in a tube furnace at 350 °C for 3.0 h and at 1000 °C for 2.0 h [26]. After carbonization, the modified wood was labeled NiFe/CW (carbonized birch wood doped with NiFe NPs). The electrode prepared without metal doping is denoted as CW. The electrical conductivity of both electrodes was tested [26].

Scanning electron microscopy (SEM; Hitachi, Japan) was used to study the morphology, pore shape and metal particle distribution characteristics on the surface of the NiFe/CW electrode. The specific surface area and pore size of NiFe/CW were analyzed using an automatic physical adsorption instrument (BET; Quantachrom, U.S.A.). The elemental composition of NiFe/CW was analyzed using scanning transmission electron microscopy (STEM; Czech FEI, Czech) in combination with energy dispersive X-ray spectroscopy (EDX). The crystallization of the NiFe/CW metal alloy after carbonization was examined using an X-ray diffractometer (XRD; Tongda, China) at 20.0–80.0° (2θ). Furthermore, the metal content in NiFe/CW was analyzed by X-ray photoelectron spectroscopy (XPS; Esca Laboratory 250 Xi, measured by Guangzhou Quality Testing Technology Service Co., Ltd, China). The conductivity setup is a four-point probe setup (Ossila Ltd., UK) and the used software Sheet Resistance (v. 2.0.3.0, Ossila Ltd., UK). Using a Nuclear Magnetic Resonance (NMR) spectrometer to analyze the changes in H spectrum of an emulsion before and after its demulsification (AVANCE NEO 400 MHz, Bruker).

2.2. Methods for the preparation and characterization of emulsions

2.2.1. Preparation of emulsions/microemulsions

Toluene (>99.5 %) was used as the oil phase of the emulsions and microemulsions, and various types of surfactants were used as stabilizers.

The concentrations of all surfactants in the toluene emulsion were controlled at 0.50 g/L. The specific configurations were as follows: polyethylene glycol sorbitan monolaurate (Tween-20) (>96 %, nonionic surfactant, hydrophilic-lipophilic balance = 16.7, Solarbio, China) was used to stabilize toluene emulsions with toluene volume fractions of 1 % and 5 %; sodium dodecyl sulfate (SDS) (95 %, anionic surfactant, hydrophilic-lipophilic balance = 40.0, Solarbio, China) was used to stabilize toluene emulsions with a toluene volume fraction of 1 %; and cetyl-trimethylammonium bromide (CTAB) (99 %, cationic surfactant, hydrophilic-lipophilic balance = 15.8, Solarbio, China) was used to stabilize toluene emulsions with a toluene volume fraction of 1 %. The surfactant was dissolved in the oil phase, and the aqueous phase was slowly added under stirring. The mixture was stirred at 1500 RPM for 0.5 h and ultrasonicated for 0.5 h to prepare the toluene emulsion. Emulsions with low oil contents are relatively stable [30]. The diluted emulsions showed no spontaneous demulsification when allowed to stand for over 3.0 d.

The 1 % toluene microemulsion was prepared using Tween-20 as a stabilizer and 1-butanol (AR, SCR, China) as a co-solvent. The volume ratio of toluene:Tween-20:1-butanol: water was 44.2:4:0.8:1. First, Tween-20 was mixed with 1-butanol and stirred thoroughly. Then, ultrapure water was added. Finally, toluene was added slowly, the solution started to become turbid, and stirring was continued until the liquid was stratified. The lower layer of the light blue liquid was the 1 % toluene microemulsion.

2.2.2. Characterization of toluene and emulsions

The O/W droplet states were monitored during demulsification using optical microscopy (Soptop, China). An ultraviolet (UV)–visible (Vis) spectrophotometer (Shimadzu, Japan) was utilized to measure the transmittance and toluene content of the samples post-demulsification. Toluene solutions were prepared with methanol as the solvent at various concentrations. Scanning was performed in the 200–400 nm UV wavelength range, and the absorption peak at 261 nm was confirmed to correspond to the characteristic absorption peak of toluene (Fig. S1a, Supporting information). Then, the absorbance value of toluene at 261 nm was measured for solutions with varying concentrations, and a standard curve of toluene concentration vs. absorbance was generated with an R^2 value of 0.9988 (Fig. S1b, Supporting information). The standard curve was used to calculate the toluene content in the solutions after demulsification. A high-speed camera (iX-Cameras, U.K.) was employed to capture the dynamics of toluene adsorption by the electrodes.

During the experiment, as demulsification progressed, the transparency levels of the emulsions/microemulsions gradually increased. Transmittance in the visible range was highly correlated with the degree of demulsification for the emulsions/microemulsions. Therefore, transmittance was employed to quantify the degree of demulsification of the emulsions/microemulsions. The transmittance spectra of the emulsions were monitored over time in the 200–800 nm range. The transmittance at 700 nm was utilized to assess the degree of demulsification (Fig. S2, Supporting information). Before the demulsification experiment, the transmittance of ultrapure water was adjusted to 100 % at 700 nm. Emulsions with a concentration of 1 % were subjected to voltages of 1.0 V, 1.2 V and 1.5 V, and 5 % emulsions were treated with a voltage of 1.5 V and 5.0 V. The 1 % microemulsion was treated with a voltage of 5.0 V.

In the experiment, when the transmittance of the sample at 700 nm reached 90 %, it indicated complete clarification of the emulsion/microemulsion. Moreover, under this condition, no O/W droplets were observable under the microscope, and the toluene removal efficiency surpassed 90 %. Therefore, a transmittance of 90 % was adopted as the criterion for complete demulsification.

2.2.3. Toluene removal efficiency (η)

$$\eta = \frac{V_a - V_b}{V_a} \tag{1}$$

where V_a is the initial concentration of toluene in the emulsion (V/V) and V_b is the concentration of toluene after complete demulsification.

2.2.4. Specific energy consumption calculation

The specific energy consumption (*SEC*) in Equation (2) is defined as the electrical energy required to adsorb 1 kg of toluene in wastewater at the electrode (kWh) [31–33].

$$SEC = \frac{10^3 E}{V\rho\eta V_a} \tag{2}$$

In the above formula for calculating *SEC* (kWh kg^{-1}), E is the consumed electric energy (kWh), V is the volume of the sample (mL), ρ is the density of toluene (0.87 g cm^{-3}), and η is the removal efficiency of toluene.

2.3. Preparation of the demulsification experiment

As shown in Fig. 1, two NiFe/CW electrodes were arranged in parallel, connected by copper wires, and separated by a 1.5 mm thick insulating gasket. The total mass of both electrodes was approximately 0.65 g. Three groups were set up: an experimental group, a control group, and a blank group. The experimental samples were measured with applied voltages and electrodes, the control samples were tested with electrodes and without applied voltage, and the blank samples remained free from electrodes and voltages. A parallel control test was employed to evaluate and compare the electro-demulsification properties of the electrode. An Ivium electrochemical workstation (IVIUM Technologies, Netherlands) controlled by a computer was connected to copper wires on the electrode via electrode clips; the electrode was inserted vertically into the reactor containing 18 mL of the emulsion. The sampling port was set and sealed. Two copper wires and the sampling port protruded from three holes on the cap to avoid evaporation of the emulsion. The demulsification experiments were conducted under magnetic stirring (100 RPM, JD, China). Given that demulsification can be achieved using a single electrode, a similar experiment was performed with a single electrode (Fig. S3, Supporting information).

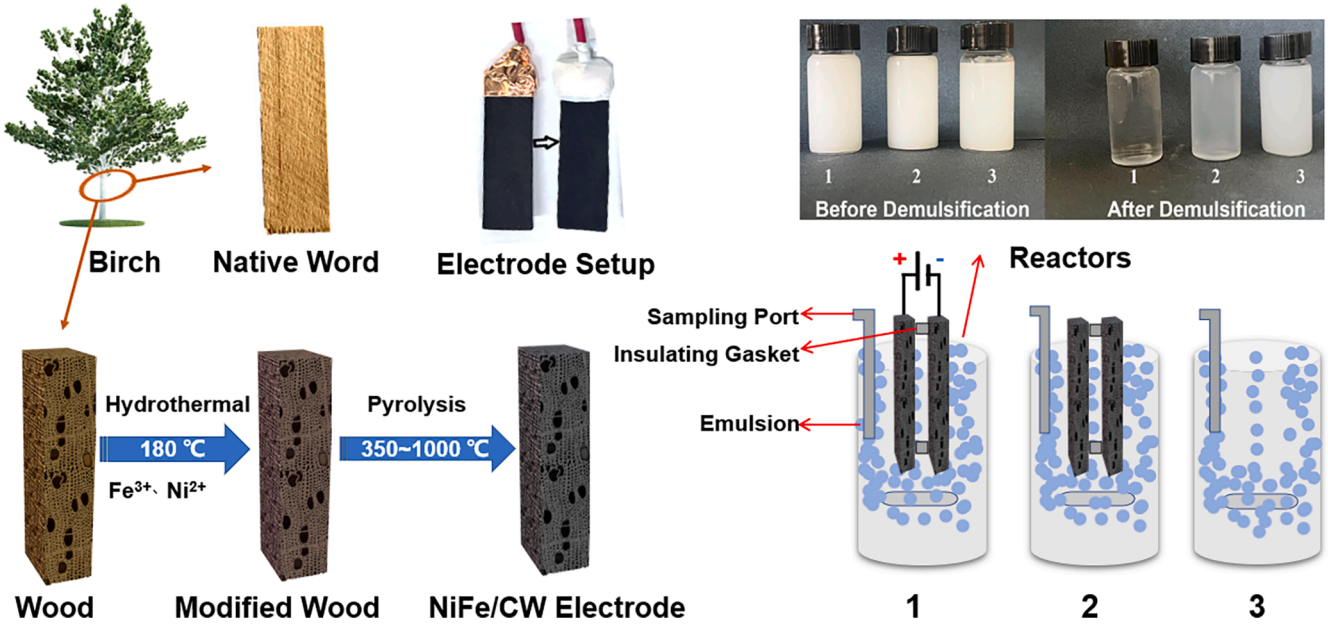

Fig. 1. Schematic diagram of the demulsification experiment: 1, 2 and 3 represent the experimental group, control group and blank group, respectively.

2.4. DFT analysis method

To gain deeper insight into the process and mechanism of electro-demulsification and the removal of organic matter by biomass electrodes, a $C_{54}H_{18}$ graphene model with 19 benzene rings was used to represent a pure graphene electrode (Fig. S4a, Supporting information). All carbon atoms were sp^2 hybridized, and each carbon atom bonded with three other carbon atoms, forming a honeycomb polygon. The edges of the model were balanced with hydrogen atoms, and the graphene system had a closed-shell electronic configuration [34]. However, the pyrolysis of biomass normally forms graphene-like substances (biomass model, $C_{57}H_{16}O_8$) with some acid functional groups (Fig. S4b and S4c) [35], namely, lactone, phenol, lactol, and carboxyl groups (Fig. S4b, Supporting information) [35,36]. The $C_{54}H_{18}$ graphene model was used to represent a pure graphene electrode, and the $C_{57}H_{16}O_8$ char model was used to simulate the biomass electrode. To study the adsorption process, a statistical physics theory was built with two hypotheses: (i) the solution was an ideal solution and (ii) there were no mutual interactions between the adsorbent (i.e., NiFe/CW) and solvent (i.e., water) [35].

Both simplified electrode models (Figs. S4a and Fig. S4b) were utilized in the density functional theory (DFT) calculations. Becke's gradient-corrected exchange–correlation, the Lee–Yang–Parr correlation functional, and Grimme's D3 dispersion correction (B3LYP-D3) were used. This functional delivered an excellent compromise between computational time and electronic properties, such as electronic energies, vibrational frequencies, and structural information, in previous studies [37–43]. In all calculations, the "Gen" keyword was used. To improve the computational efficiency, C, H, and O atoms adopted the 6-311G (d, p) method, and the Los Alamos National Laboratory (LANL) effective core potentials (ECPs) with the appropriate valence double-zeta basis set (LANL2DZ) were used for metal atoms (Ni, Fe). The geometrical minima were confirmed by vibrational analysis without imaginary frequencies. The zero-point vibrational energy (*ZPVE*) was obtained in the frequency calculations to correct the electronic energies. All calculations were performed using the Gaussian 09 Revision E.01 suite of programs [43].

The binding energy (*BE*) between the adsorbent surface and the adsorbate species was obtained using the following equation [44]:

$$BE = E_{total} - (E_{adsorbate} + E_{adsorbent}) \quad (3)$$

Where E_{total} is the total electric energy of the system after adsorption, $E_{\mathrm{adsorbate}}$ is the electric energy of the adsorbate species, and $E_{adsorbent}$ is the energy of the adsorbent surface.

Finally, the adsorption of toluene on the electrode, the effect of the doped metal, and the effect of the electric field on adsorption were analyzed by DFT calculations and models.

3. Results and discussion

3.1. Structure and morphology of the electrode

In our previous work [26], the synthesis of the NiFe/CW electrode was comprehensively studied; this synthesis involves two critical steps (Fig. 1). First, metal cations such as Ni^{2+} and Fe^{3+} are introduced into native wood through a hydrothermal treatment process, allowing them to permeate the hollow pores of the wood. Subsequently, controlled pyrolysis is employed with varying temperature gradients. To initiate the process, a carbonization temperature of 350 °C is employed to facilitate metal nucleation, thereby promoting the development of metallic crystals and a graphitic structure. Subsequently, the temperature is gradually raised until it reaches 1000 °C. These steps are critical for the production of a self-standing electrode, as they prevent the carbon from becoming brittle and ensure the retention of high electronic conductivity.

Figs. 2 and 3 show the physical characterization results of the biomass electrodes following hydrothermal treatment and carbonization. The SEM images of the NiFe/CW electrodes (Fig. 2a–2c) show honeycomb-like pores that are similar to the original 3D pore structure of wood. Some particles were attached to the cell walls of the electrode pores (Fig. 2b), and these particles were nanorod shape (Fig. 2c). These particles were identified as doped NiFe NPs on the basis of transmission electron microscopy (TEM) elemental mapping (Fig. 2e–2i). The XRD pattern corresponded to a face-centered cubic crystal structure with 2θ values of 44.2°, 51.5°, and 75.8°, corresponding to the (1 1 1), (2 0 0) and (2 2 0) crystallographic planes (Fig. 3a). The main product was nickel iron ore ($FeNi_3$). Further XPS analysis of the metals Fe and Ni revealed that the characteristic peaks of Fe $2p_{3/2}$ and Ni $2p_{3/2}$ were located at 707.0 eV and 853.1 eV, respectively (Fig. 3b, 3c). This indicates that Ni and Fe primarily existed in the form of metals and minor metal oxides [26,45,46]. The atomic content analysis by XPS results indicated an approximate total metal atomic percentage of 3.2 % (Fig. 3d), with carbon constituting 88.4 % and oxygen comprising 5.7 %. The C_{1s} spectrum XPS results for the samples are shown in Fig. 3e and Fig. S5. Carbon atoms differ in their binding energies depending on whether they are linked to one oxygen atom by a single or double bond or to two oxygen atoms [47]. The main peak at 284.7 eV corresponds to sp^2 hybridized C = C bonds, while the peaks at 287.2 and 288.9 eV are attributed to bonding with oxygen atoms [26]. The FT-IR spectrum of the biochar is shown in Fig. 3f. The most obvious peak was at 3430 cm^{-1}, which is related to hydroxyl groups on the biochar surface [48]. The peak at 2820 cm^{-1} can be attributed to C-H in alkanes, indicating the existence of aliphatic structures in the biochar [49]. In addition, the absorption peak at 1631 cm^{-1} represents the carbonyl functional group in conjugated olefins [50,51]. The absorption peak at 1590 cm^{-1} represents the stretching vibration of C = C [49]. The signal at 1080 cm^{-1} comes from the stretching of the C-O group in esters and phenols [52,53]. These acidic functional groups can serve as binding sites for the adsorption of organic compounds. The peak corresponding to the bending vibration of the C-H bond in olefins can be observed at 989 cm^{-1}. Additionally, the π-π* transition indicates the presence of aromaticity in the electrode. The porosity of NiFe/CW was analyzed by the nitrogen adsorption method, and the obtained Brunauer–Emmett–Teller (BET) surface area was 387 m^2/g [26]. The pore size distribution diagram confirmed that the surface porosity of the carbonized birch is mainly characterized by micropores (Fig. 3g), and the isotherm of the NiFe/CW electrode exhibits a typical type IV hysteresis curve (Fig. 3h), indicating the presence of mesopores in the electrode [26,54]. The multiscale porous structure of the electrode material, especially the well-developed micropores, significantly contributes to the removal of emulsions and organic compounds.

3.2. Electro-demulsification experiment

3.2.1. Demulsification of the 1 % toluene–Tween-20 emulsion

The novel electro-demulsification method, utilizing carbonized birch as a self-standing electrode, was initially developed. To assess its feasibility, Tween-20-stabilized emulsions containing 1 % toluene were subjected to three different voltages: 1.0 V, 1.2 V, and 1.5 V. Fig. 4a illustrates that demulsification was most effective in the experimental sample subjected to an electric field, resulting in over 90 % transmittance in 5.0 h. In contrast, the control sample reached only 50 % transmittance, and the blank sample had the lowest transmittance, approximately 10 %. In summary, the demulsification effectiveness follows this order: experimental group > control group > blank group. A transmittance of 90 % was adopted as the criterion for complete demulsification (vide supra). A comparison of the transmittance at different voltages revealed that demulsification at 1.5 V achieved 90 % transmittance in 2.3 h, whereas at 1.2 V, it took 4.3 h, and at 1.0 V, the process required 4.7 h. The toluene removal efficiency was shown in Fig. 4b. At 1.5 V, the toluene removal efficiency reached 99.13 %. The performance data was summarized in

Table 1
Comprehensive analysis of the demulsification effect when the transmittance of the emulsion reaches 90%.

Groups	[a] t (h)	[b] E (kWh)	[c] q (mg g^{-1})	[d] SEC (kWh kg^{-1})
1.0 V–1 % Emulsion–Tween-20	4.7	1.76×10^{-6}	236	0.011
1.2 V–1 % Emulsion–Tween-20	4.3	2.31×10^{-6}	237	0.015
1.5 V–1 % Emulsion–Tween-20	2.3	5.56×10^{-7}	239	0.004
5.0 V–5 % Emulsion–Tween-20	3.4	1.19×10^{-5}	1180	0.016
5.0 V–1 % Microemulsion–Tween-20	6.9	1.85×10^{-4}	226	1.259
1.5 V–1 % Emulsion–SDS	3.2	4.22×10^{-6}	238	0.027
1.5 V–1 % Emulsion–CTAB	3.5	4.60×10^{-6}	237	0.030

[a] t is the time required for the transmittance of the emulsion to reach 90%, [b] E is the consumed electric energy, which was obtained from Ivium software, [c] q is the adsorption capacity of the electrode, and [d] SEC is the specific energy consumption.

Table 1 and Table S1. The demulsification experiment at 1.5 V exhibited a high toluene removal efficiency and low electricity consumption, requiring only 5.56×10^{-7} kWh to achieve complete demulsification. Additionally, increasing the voltage reduced the *SEC* from 0.011 kWh kg^{-1} to 0.004 kWh kg^{-1}, demonstrating the advantage of demulsification at 1.5 V. Therefore, when treating 1 % emulsions, using 1.5 V for demulsification offers additional advantages. The electrode was cycled five times. Nevertheless, the demulsification ability diminished (Fig. S6, Supporting information). This phenomenon is likely attributed to the adsorption of high-molecular-weight surfactants onto the electrode, resulting in the clogging of electrode pores. Additionally, it may be associated with the potential collapse of the pore structure during operation. Future endeavors will be directed towards enhancing the durability of the electrode.

The distribution and state characteristics of O/W droplets in the emulsion during demulsification at 1.5 V were observed with an optical microscope (Fig. 5). Initially, no voltage was applied, and the field of view was filled with droplets below 5.0 μm in size. With the continuous application of voltage, the number of droplets gradually decreased; at 2.0 h, the droplets in the field of view almost completely disappeared. Overall, considering the motion of the emulsion under the electric field (Video S1), there was no noticeable droplet coalescence. Furthermore, the droplet size remained relatively constant, but the number of droplets decreased as the experiment progressed (Fig. 5). Consequently, the electric field force did not cause noticeable coalescence of the droplets. Additionally, However, it did facilitate the adsorption and accumulation of polarized molecules within the electrode's pores, potentially resulting in demulsification processes occurring within the electrode. Therefore, the increase in emulsion transmittance is primarily attributed to the reduction in the number of emulsion droplets, which is mainly caused by the demulsification resulting from electro-demulsification on the electrode.

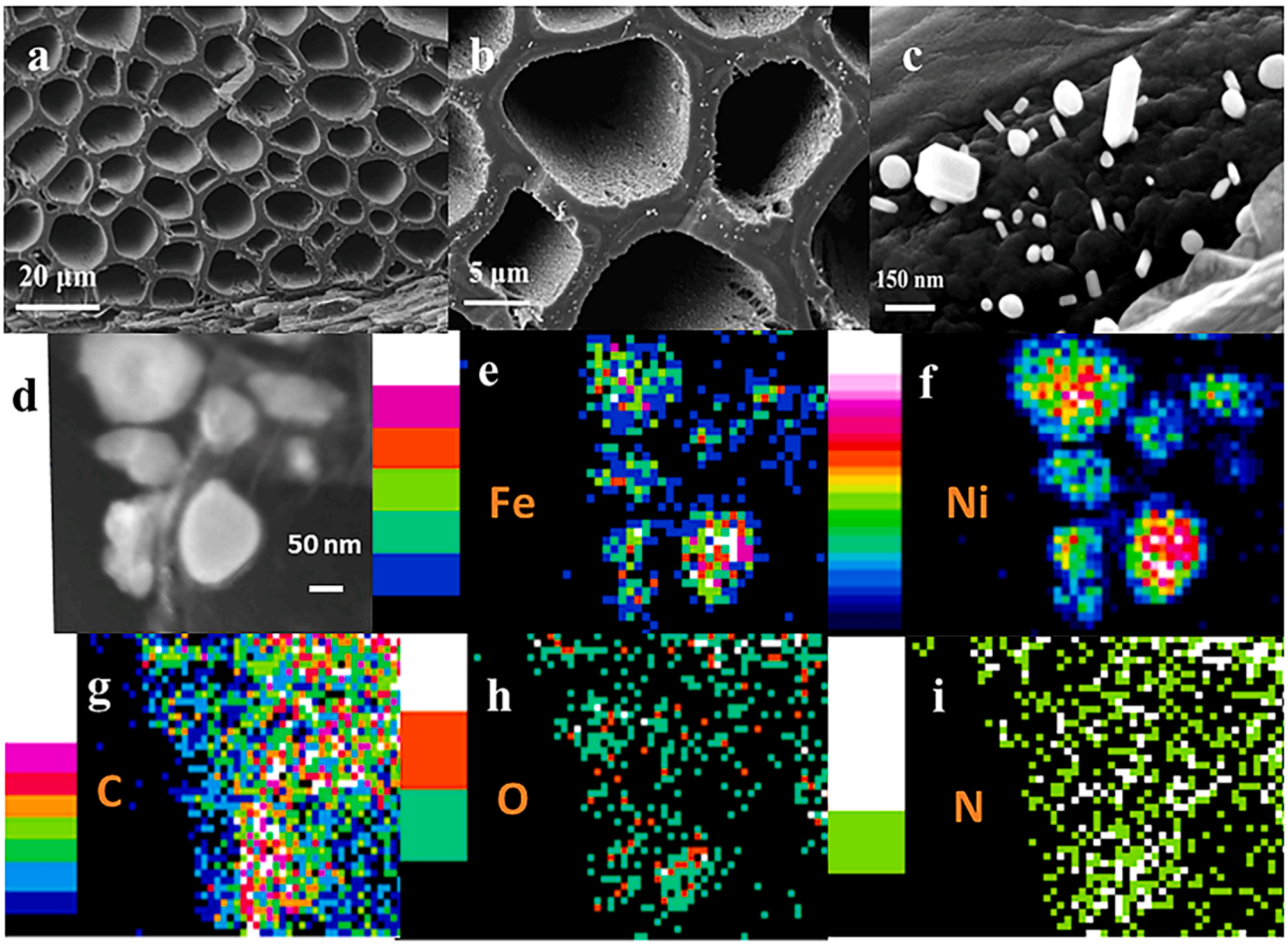

Fig. 2. Characterization of the FeNi/CW electrode. (a–c) SEM images; (d) STEM image; and (e–i) EDX mapping images.

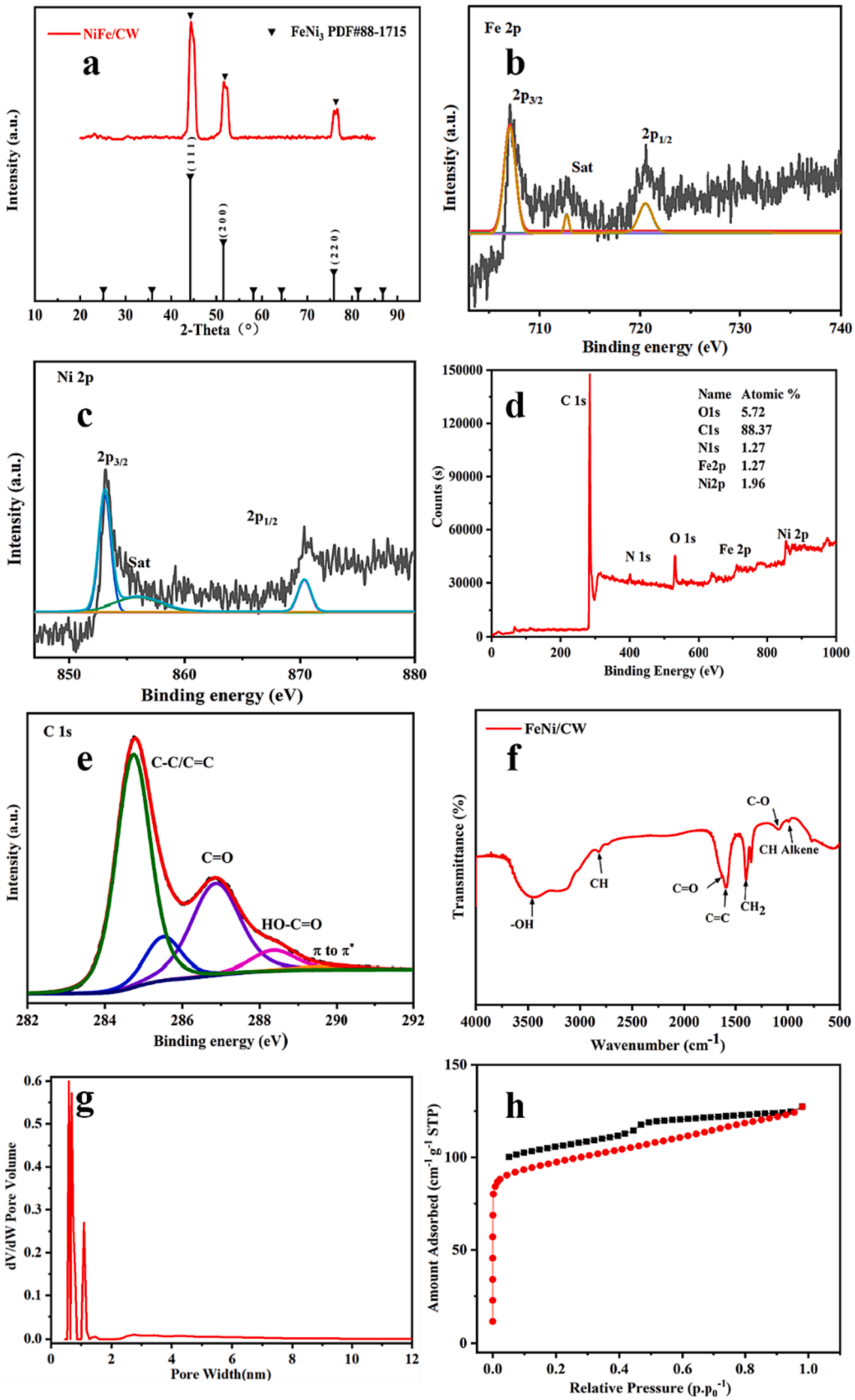

Fig. 3. Characterization of the FeNi/CW electrode. (a) XRD image; (b-c) XPS spectra of Fe 2p and Ni 2p corresponding to the electrochemical performance tests; (d) XPS survey scan spectra and surface atomic ratios; (e) FT-IR spectra; (f) XPS C 1 s spectra; (g) pore size distribution; (h) N_2 adsorption–desorption isotherm.

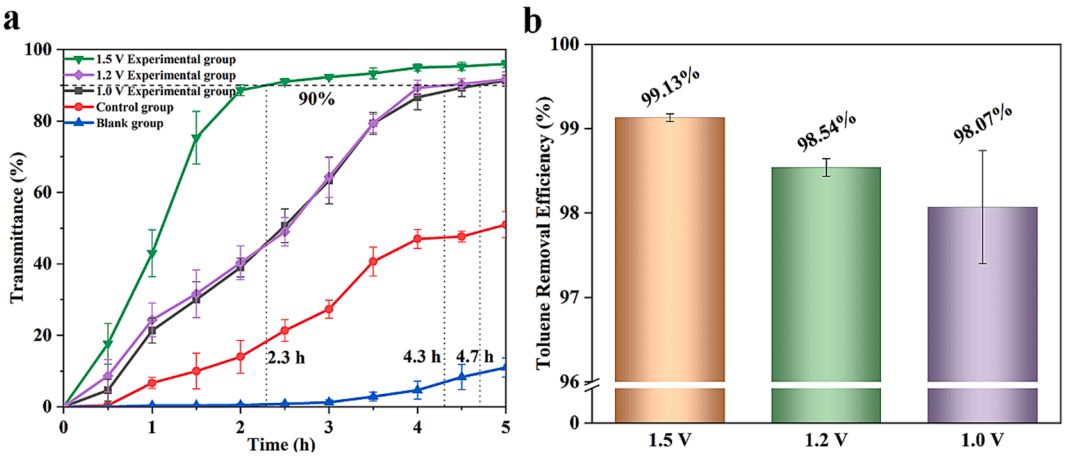

Fig. 4. (a) Change in transmission over time in the demulsification experiment with a 1% emulsion. (b) Toluene removal efficiency.

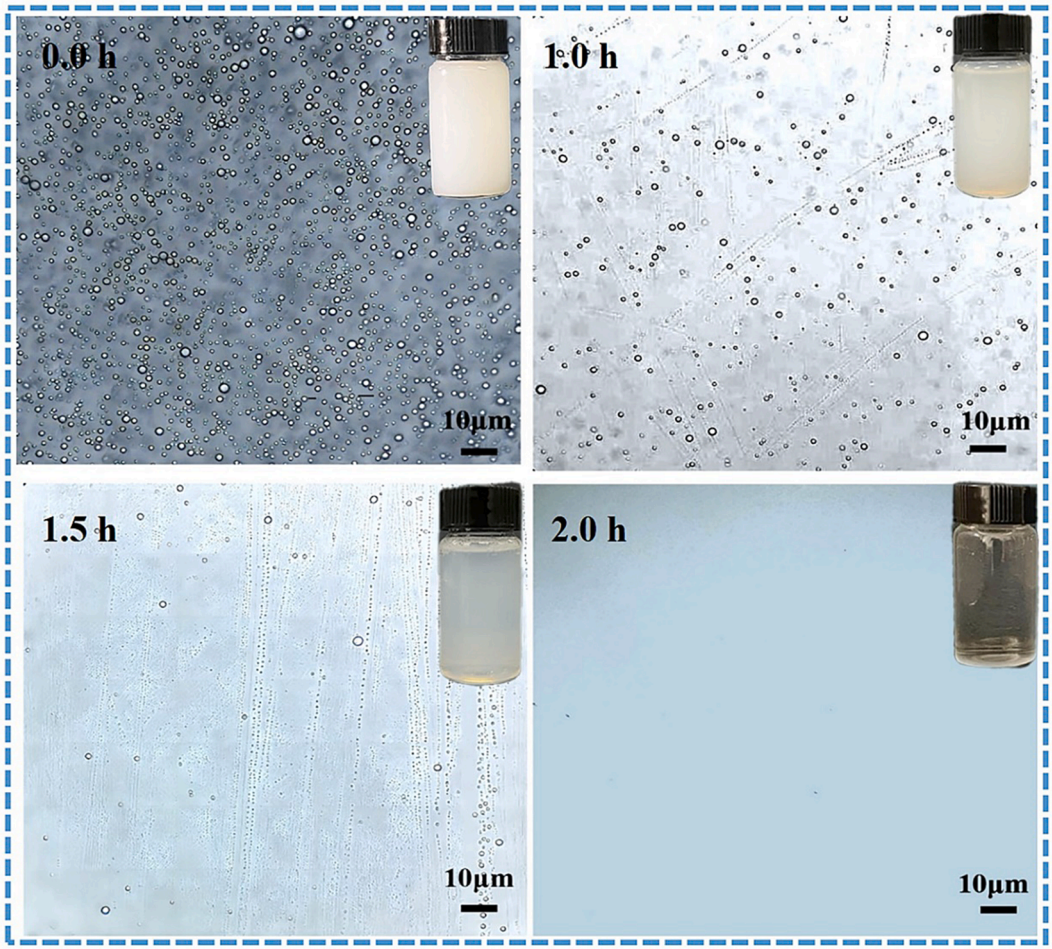

Fig. 5. Distribution of O/W droplets observed under an optical microscope during demulsification at 1.5 V and corresponding sample photographs.

To further emphasize the initial advantage of the NiFe/CW electrode in demulsification, a 1 % emulsion was treated with the CW electrode (without metal) at a voltage of 1.5 V. As shown in Fig. S7, during the demulsification process of the CW electrode, the transmittance increased slowly at first 2.5 h, and complete demulsification was not achieved until 5.9 h. At this time, the removal efficiency of toluene was 97.03 %. Due to the lack of a metal support, the CW electrode is extremely fragile and easy to break, and the surface of the electrode easily falls off during demulsification. Furthermore, our previous publication [26] characterized the electron conductivity of CW and NiFe/CW samples, revealing that NiFe/CW electrodes exhibit higher electron conductivity, with a tangential conductivity of 8.41×10^2 S/m.

3.2.2. *Demulsification of the 5 % toluene–Tween-20 emulsion*

The above experiments demonstrate that effective demulsification and toluene removal can be achieved by using low voltage at low

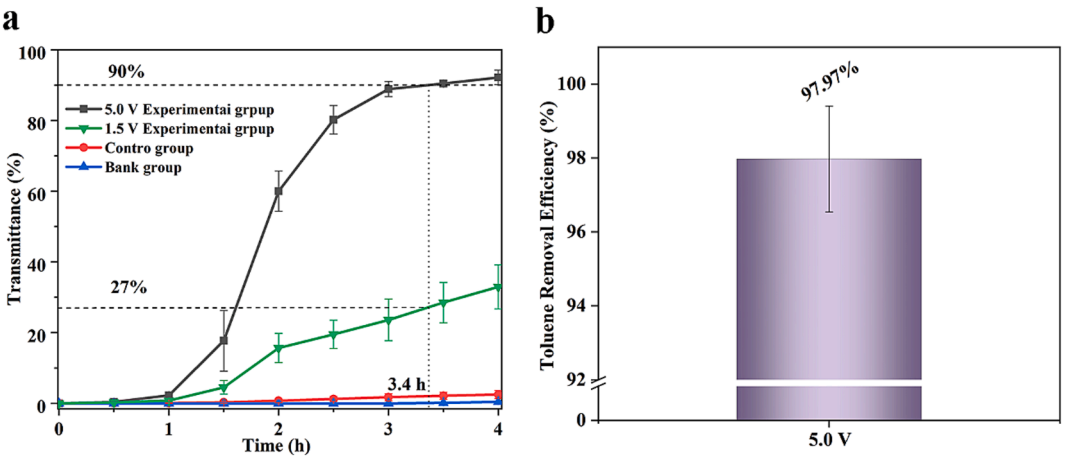

Fig. 6. (a) Change in transmission with time in the demulsification experiment of the 5% emulsion. (b) Toluene removal efficiency.

concentration. Achieving demulsification at a high concentration is of great practical significance. The demulsification processes of 5 % emulsified wastewater at 1.5 V and 5.0 V were investigated (Fig. 6). The demulsification effectiveness in the control group decreased notably at slightly higher emulsion concentrations. The demulsification process of the 5.0 V–5 % emulsion treatment was similar to that of the 1.5 V–1 % emulsion treatment, and the transmittance reached 90 % at 3.4 h. In addition, the *SEC* resulting from the 5.0 V treatment was 0.016 kWh kg^{-1} (Table 1), the removal efficiency of toluene in the emulsion was 97.97 %, and the electroadsorption capacity was 1180 mg g^{-1}. However, the experimental transmittance for 1.5 V was only 27 %. Therefore, when the concentration of the oil phase in the emulsion increases, the applied voltage can be increased to facilitate the demulsification of emulsion wastewater and the removal of toluene.

3.2.3. Effect of a microemulsion on demulsification

In the demulsification experiment of the 1 % toluene-microemulsion system, noticeable demulsification occurred when the voltage increased to 5.0 V. Figs. 7 and 8, the transmittance of the microemulsion was initially high (approximately 50 %) when a voltage was not applied, and the sample showed a blue–white color. However, only a few droplets with a diameter of less than 1.0 μm were visible under the microscope. The size of these droplets was significantly smaller than that of the toluene emulsion droplets. As the demulsification process proceeded, the microemulsion gradually changed from blue–white to milky white, and the transparency decreased significantly. The sample became milky white, and the droplets under the microscope increased in number and size; most of the droplets were of the O/W type at this time, and the high voltage was the reason for the large droplet aggregation. Afterward, the transmittance started to increase, and many large droplets disappeared from the field of view after 4.5 h. The transmittance increased to approximately 60 %, and the sample became increasingly transparent. Finally, after 6.9 h of demulsification, the transmittance reached 90 %, but the sample became completely transparent at 6.5 h. No droplets were observable under the microscope, indicating complete demulsification of the microemulsion. After 6.9 h of demulsification, the toluene removal efficiency was 93.68 %, the power consumption was 1.85×10^{-4} kWh, and the *SEC* was 1.259 kWh kg^{-1} (Table 1).

3.2.4. Effect of surfactant type on demulsification

Emulsions/microemulsions stabilized by nonionic emulsifiers were treated in the above experiments. To explore the universality of demulsification by this method, toluene water emulsions containing 1 % toluene that were stabilized by an anionic surfactant (0.50 g/L SDS) and cationic surfactant (0.50 g/L CTAB) were treated. In the 1.5 V demulsification experiments of emulsions stabilized by different ionic surfactants (Fig. 4 and Fig. 9), the change trend of light transmittance over time was almost the same among the three groups, and the light transmittance exceeded 90 % in 4.0 h. In the 1.5 V–1 % Emulsion–SDS experimental group, 98.58 % of toluene was removed after 3.2 h of

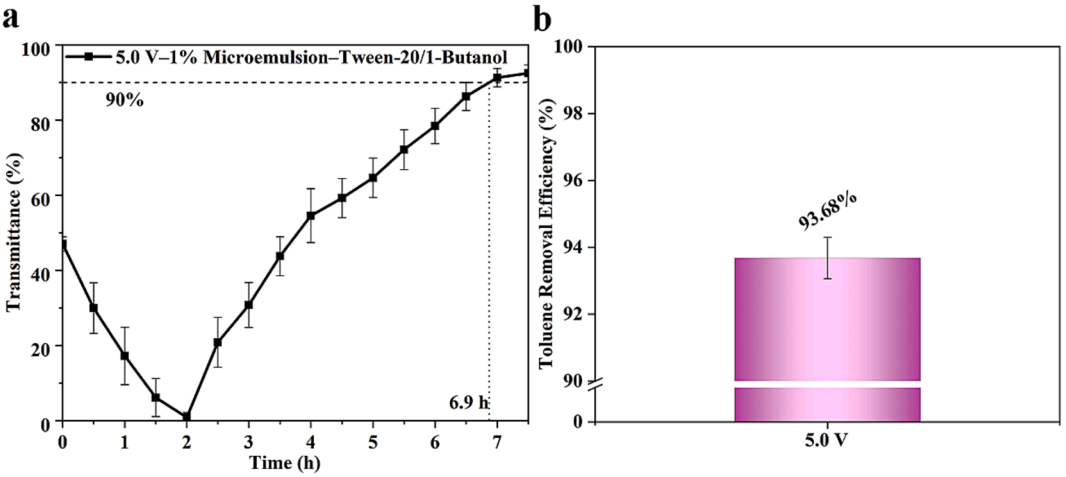

Fig. 7. Demulsification experiment of the 1% toluene microemulsion: (a) change in light transmittance with demulsification time and (b) toluene removal rate.

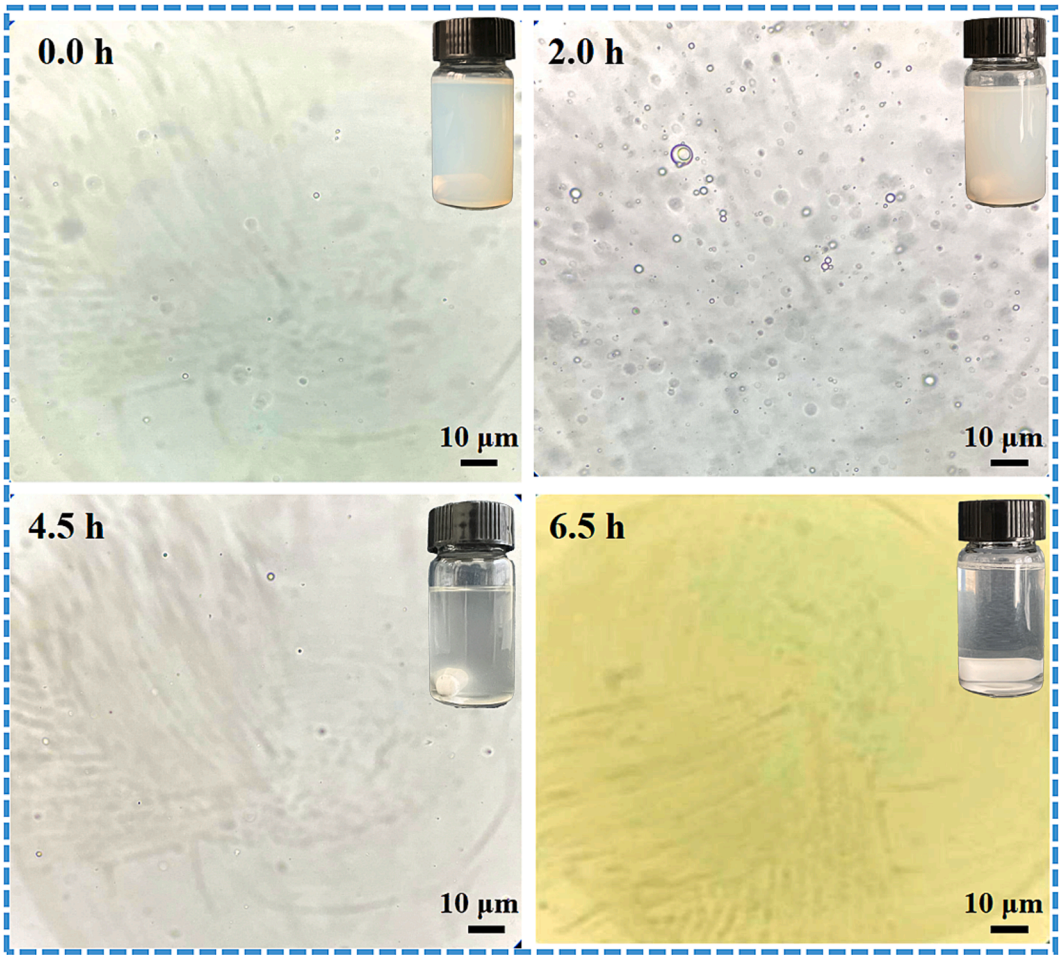

Fig. 8. Distribution and corresponding sample photos of O/W droplets under an optical microscope during the demulsification of a 1% toluene microemulsion.

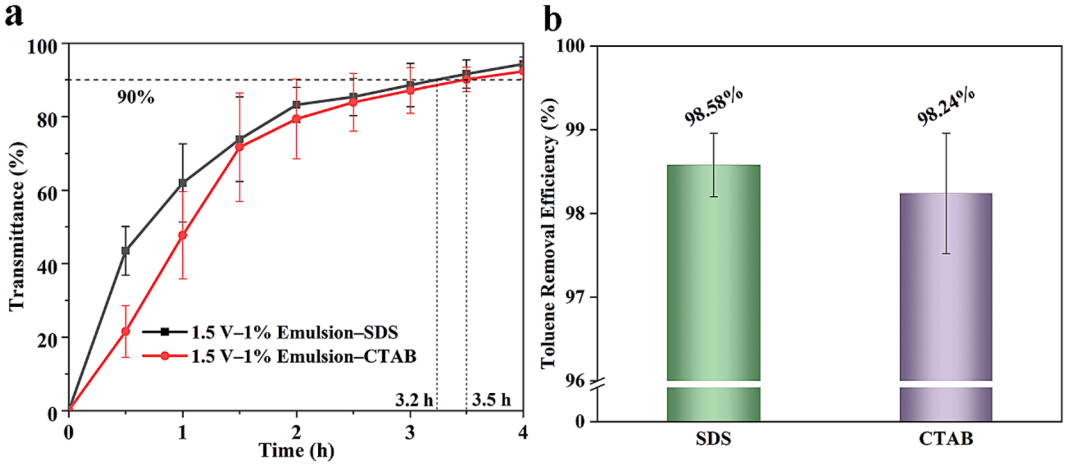

Fig. 9. Demulsification experiment of toluene emulsions stabilized by anionic/cationic surfactants: (a) change in light transmittance with demulsification time and (b) toluene removal efficiency.

demulsification. The average energy consumption was 4.22×10^{-6} kWh, and the *SEC* was 0.027 kWh kg^{-1} (Table 1). In the 1.5 V–1 % Emulsion–CTAB experimental group, the toluene removal efficiency was 98.24 %, the energy consumption was 4.60×10^{-6} kWh, and the *SEC* was 0.030 kWh kg^{-1} (Table 1). Additionally, the experiment achieves demulsification using solar energy as the power source, the result is similar to that of indoor electro-demulsification (Fig. S8).

3.3. Demulsification and oil removal mechanisms

3.3.1. Physical adsorption of toluene into the electrode structure

Graphene and graphene-like materials comprise electron-rich aromatic rings, while toluene is characterized by electron-deficient aromatic rings; as a result, π–π interactions are formed between graphene and toluene [55]. Therefore, DFT calculations were employed to

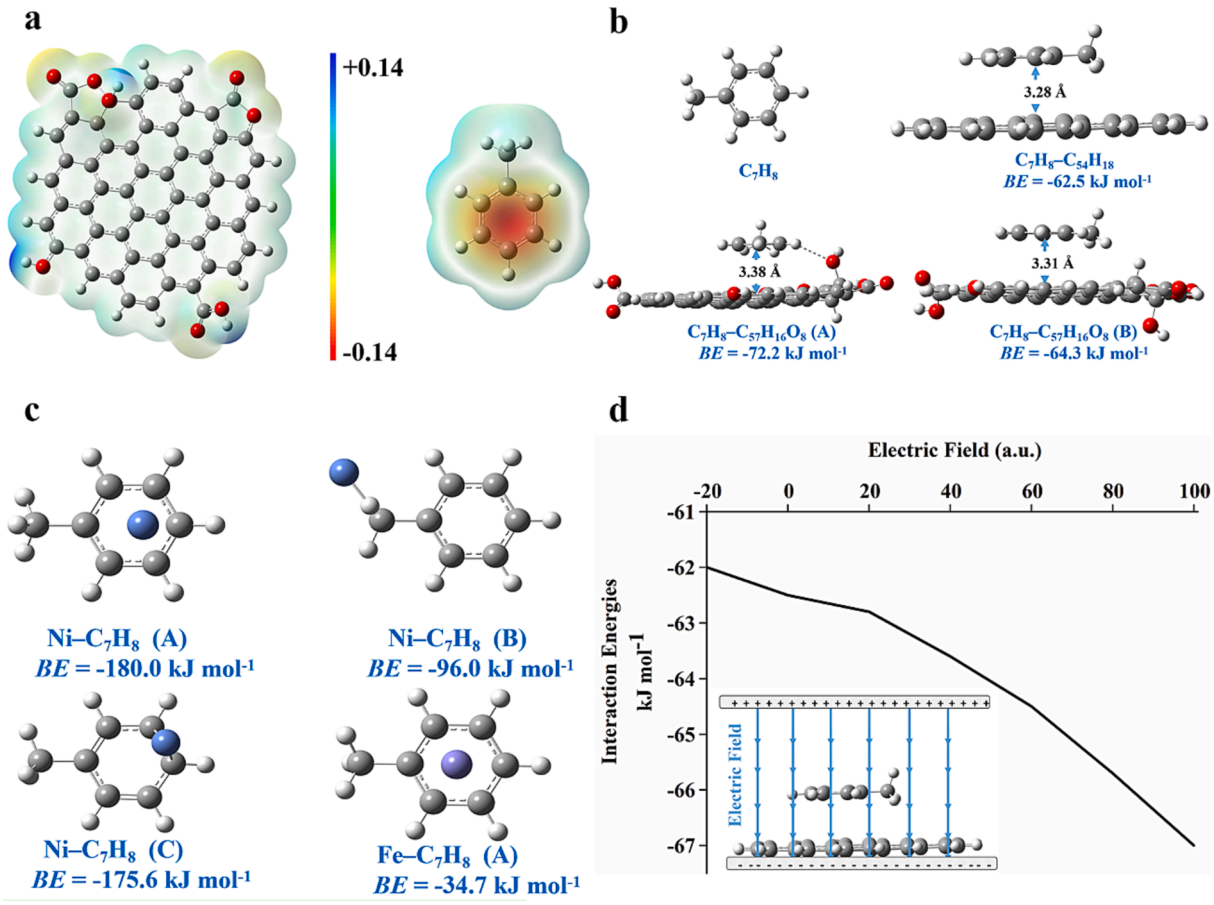

Fig. 10. (a) Electrostatic potential surfaces of $C_{57}H_{16}O_8$ and C_7H_8 calculated with DFT/B3LYP-D3. (b) Adsorption configurations of C_7H_8 and $C_{54}H_{18}$. (c) Metals interacting with C_7H_8. (d) Adsorption of C_7H_8 by $C_{54}H_{18}$ under an electric field force.

investigate the physical adsorption of toluene. Two electrode models were used in this study—the $C_{54}H_{18}$ graphene model and the $C_{57}H_{16}O_8$ biomass model—both of which contain numerous benzene rings [55,56]. The binding energies of the π–π interactions of C_7H_8–$C_{54}H_{18}$ and C_7H_8–$C_{57}H_{16}O_8$ were calculated to be −62.5 kJ mol^{-1} and −64.3 kJ mol^{-1}, respectively, as shown in (B) in Fig. 10b. The binding energy of C_7H_8–$C_{54}H_{18}$ with only π–π interactions was slightly higher than that of C_7H_8–$C_{57}H_{16}O_8$ (B). This phenomenon is due to the presence of oxygen-containing functional groups in $C_{57}H_{16}O_8$. However, the acid functional groups in the $C_{57}H_{16}O_8$ model can affect adsorption. Fig. 10a shows the electrostatic potential (ESP) diagrams of $C_{57}H_{16}O_8$ and C_7H_8; red parts represent a negative potential, and blue parts represent a positive potential. The hydrogen atoms outside the benzene ring of C_7H_8 show a high positive potential, while the oxygen-containing functional groups of $C_{57}H_{16}O_8$ show a high negative potential. Consequently, the hydrogen atoms of C_7H_8 can interact with the oxygen-containing functional groups of $C_{57}H_{16}O_8$ (C_7H_8–$C_{57}H_{16}O_8$ (A) in Fig. 10b). The corresponding binding energy is −72.2 kJ mol^{-1}. This finding suggests that the biomass electrode can adsorb C_7H_8 via π–π interactions, and the hydrogen bonding interaction between oxygen-containing functional groups in the biomass electrode and C_7H_8 can strengthen the molecular interaction between the electrode and toluene and form hydrogen bonds to promote the adsorption of toluene. An applied external voltage improves the transmission of free electrons at the negative electrode, which has a large negative potential, further promoting the adsorption of toluene by the electrode (via π–π interactions) [57].

As mentioned in the previous section, iron and nickel NPs in biomass electrode can improve the conductivity and adsorption of the electrode. The inclusion of metals leads to enhanced toluene adsorption by the electrode. Thus, the effects of metals on C_7H_8 adsorption were studied by DFT. Fig. 10c presents the binding energies of the metallic Ni and Fe clusters on the electrode surface for toluene adsorption. Three interaction modes exist for Ni–C_7H_8 interactions. In Ni–C_7H_8 (A), the interaction takes place between Ni and the benzene ring, exhibiting a binding energy of −180.0 kJ mol^{-1}, and this is the most stable configuration among the three options. In Ni–C_7H_8 (B), an interaction occurs between Ni and the CH_3 group of toluene (BE = -96.0 kJ mol^{-1}). For Ni–C_7H_8 (C), the Ni atom interacts with carbon atoms on the benzene ring (BE = -176.0 kJ mol^{-1}). However, there is only one Fe with a binding energy of −34.7 kJ mol^{-1} (Fe–C_7H_8 (A) in Fig. 10c). In general, electrodes with mixed metals can enhance the adsorption of toluene. According to the binding energy results, Ni can enhance the adsorption of toluene more than Fe can.

Finally, the mechanism of electrode removal of toluene in wastewater at the microscopic level was further assessed by modeling graphene in an electric field. In this study, an electric field can be formed around the electrified electrode, and toluene in the aqueous phase is affected by the electric field force. Therefore, to explore the effect of the electric field between the electrodes on the adsorption of toluene on the electrodes, a model of toluene adsorption on the electrodes under the effect of the electric field force was constructed, as shown in Fig. 10d. Due to π–π interactions, toluene is preferentially adsorbed on the electron-rich negative electrode. With increasing electric field force, the binding energy between toluene and the electrode decreases gradually and is lower than that without an electric field (BE = -62.5 kJ mol^{-1}). Therefore, toluene dissolved in the aqueous phase is subjected to electric field forces, which promote the adsorption of toluene on the electrode.

3.3.2. *Process of demulsification and oil removal*

Ionic surfactants impart an electrical charge to the emulsion. resulting in electrophoretic migration toward the oppositely charged

electrode upon the application of voltage. In contrast, nonionic surfactants typically lack this charge-inducing property. To further investigate the demulsification mechanism, we will comprehensively examine the demulsification and oil removal processes of toluene emulsion droplets stabilized by Tween-20. The change in COD in the emulsion at various time points during the electro- demulsification experiment (Fig. S9), reveal a significant decrease in organic material, amounting to a remarkable 96.33 % removal.

Furthermore, pure toluene adsorption experiments were conducted, with concentrations and time varied (Figs. S10, S11; Tables S2, S3). In contrast to electro-demulsification, applying a 1.0 V voltage to toluene aqueous solution showed only a slight initial improvement in pure adsorption, especially without surfactant (Fig. S11). Compared to pure adsorption, the 1.0 V-treated toluene solution did not exhibit the same advantage as in demulsification (Fig. S11). This suggests simultaneous demulsification and adsorption, with efficient toluene removal depending on its oil–water droplet form. The electric field accelerates charged toluene droplets into electrode pores during demulsification, enhancing adsorption. Therefore, toluene removal is optimized when it exists in the oil–water droplet form.

Video S2 (Supporting information) was recorded using a high-speed camera to illustrate the motion of floating oil on the emulsion surface

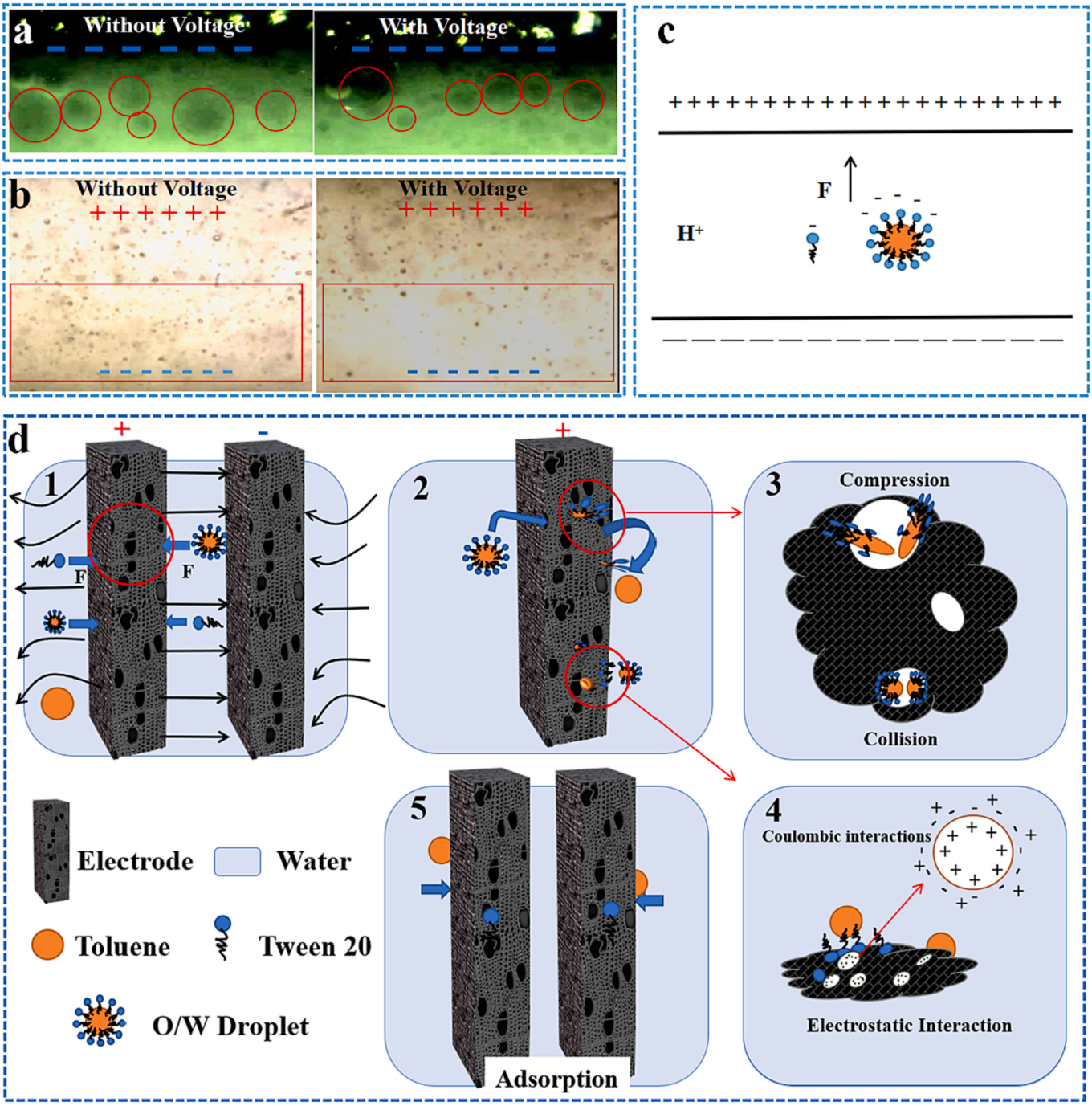

Fig. 11. (a) Floating oil droplets under a high-speed camera (the cathode is located above the upper border of the image). (b) States of O/W droplets in an electric field (the emulsion was dripped between the two electrodes). (c) Electrophoresis of O/W droplets in an electric field. (d) Schematic diagram of the electro-demulsification and adsorption removal of organic matter (Tween-20 and toluene) by a biomass electrode.

before and after the application of voltage in the demulsification experiment. Fig. 11a shows a screenshot from Video S2. After applying a voltage, the floating oil near the electrode began to move and accelerate toward the electrode. The movement of the floating oil was caused by mass transfer, indicating the adsorption of toluene by the electrode. In the experiment, the O/W droplet was capable of moving in the electric field, as demonstrated in Video S1. Fig. 11b provides a screenshot from Video S1 (Supporting information). The droplet exhibited Brownian motion before the application of voltage. Subsequently, when a voltage was applied, the droplet initiating movement toward the positive pole, resulting in a decrease in concentration at the cathode and an increase at the anode. To determine the mechanism of droplet movement in the electric field, several groups of electrodes were prepared, as shown in Fig. S12 (Supporting information), and the electrophoretic effects of O/W droplets in the electric field were determined. The mechanism behind the formation of O/W droplets is elucidated in Fig. 11c. The hydrophobic terminals of the Tween-20 molecules surround toluene molecules, while the hydrophilic terminals, consisting of oxygen-containing functional groups, remain in the aqueous phase. The analysis of the composition of the emulsion reveals that the hydroxyl groups in Tween-20 are responsible for the highly electronegative status of the droplets and Tween-20. The initial pH of the emulsion was 5.5, indicating that the hydrogen atoms on the hydroxyl groups in the Tween-20 molecule were ionized. Therefore, the O/W droplets and Tween-20 in the aqueous phase were polarized and electrophoresed to the anode under the action of an electric field.

The demulsification and oil removal processes that took place in the experiment are depicted in Fig. 11d. An electric field is formed around the energized electrode, polarizing the nearby charged particles (Tween-20, O/W droplet) and accelerating them toward the anode in electrophoretic motion, especially the particles between the electrodes, and these particles collect near the electrode. The high surface area of pores significantly extends the electric double layer (EDL), enhancing the material's adsorption capabilities associated with a large number of Coulombic forces [58]. Under the influence of an electric field force, O/W droplets that enter the electrode pores collide and compress each other. This disrupts the rigid film of the droplets at the oil–water interface [59]. The increased instability of the droplets ultimately leads to disruption of the emulsion and the release of toluene [60]. The multiscale pores of the electrode provide ample space for demulsification. The electric field force is the main cause of demulsification. As toluene exists in the form of O/W droplets, the electric field compels these droplets into the electrode pores. Subsequent to the breaking of these droplets within the pores, the released toluene exhibits a significantly increased contact area with the electrode. This heightened contact area is the primary factor contributing to the elevated removal efficiency of toluene. In addition, Tween-20 molecules on the surface of the droplets are attracted to the charged electrode (electrostatic interaction) and pulled away from the droplet surface, leading to destabilization of the O/W droplets and the release of toluene [14,15]. Under the disturbance of microbubbles produced by water electrolysis, the collision frequency between O/W droplets and between O/W droplets and the electrode is relatively high, reducing the resistance between O/W droplet films (electrostatic repulsion) and promoting the electro-demulsification of particles. Last, the rich micropore structure of the electrode provides a very large surface area for the adsorption of pollutants. Small molecular organics can be adsorbed on the surface and inner pore walls of the electrode through surface adsorption and micropore filling [61,62], and the main mechanism of toluene adsorption is π-π interactions [16,17]. The electrode further reduces the concentration of organic matter in the emulsion by adsorbing free toluene and Tween-20, facilitating the demulsification process [15,63]. The pH after demulsification increased from 5.5 to 6.8, confirming the removal of Tween-20.

3.3.3. Mechanism of demulsification and oil removal

In the experiments and DFT calculations, several key observations and characteristics were identified related to the NiFe/CW electrode. These phenomena included demulsification effects, toluene adsorption, the motion of floating oil, and the behavior of droplets in an electric field. Based on the experimental results and analysis, the mechanisms behind demulsification and oil removal can be summarized as follows: 1. The electric field force and multiscale porous structure of the electrode lead to demulsification. The electric field polarizes the O/W droplets and propels them toward the anode through electrophoresis. Ultimately, they accumulate on the electrode surface and diffuse into the pores of the electrode. Due to confinement within the finite space of the microporous structure of the electrode, the droplets compress and interact, ultimately leading to the rupture of the rigid film. 2. Electrostatic interaction: Electrostatic interactions between the electrode and O/W droplets lead to the detachment of Tween-20 from the droplet surface, resulting in disruption of the emulsion. Furthermore, there are π–π interactions between toluene and the electrode, leading to a reduction in the oil concentration in the emulsion. Thus, demulsification and oil removal primarily result from several factors, including the electric field force electrostatic interaction, multiscale porous structure, large specific surface area, excellent electrical conductivity, specific oxygen-containing functional groups, and nickel–iron adsorption docking points.

Given the unique characteristics of the electrodes, electrochemical reactions may occur. Therefore, 1 M KOH electrolyte solution was used as a solvent before demulsification. Toluene-saturated solution, 0.50 g/L Tween-20 solution, and a 1 % toluene emulsion stabilized by 0.50 g/L Tween-20 were prepared at room temperature. Ag/AgCl was used as the reference electrode. Cyclic voltammetry was performed at different scanning speeds. Cyclic voltammetry was used to assess the treatment of 1 % toluene solution with different concentrations of Tween-20. However, no obvious redox reactions were observed (Fig. 12a-12d). Nuclear magnetic resonance (NMR) and infrared spectroscopy analysis were conducted on the wastewater samples before and after demulsification, but no new substances were found to be formed (Fig. 12e-12f). Moreover, the outer layer of the O/W droplets consisted of Tween-20 or other surfactants, which are not prone to facile redox reactions. The molecular structure of surfactants typically comprises a hydrophilic (water-attracting) head group and a hydrophobic (water-repelling) tail group. This arrangement enables surfactants to serve as interface agents between water and oil, facilitating the dispersion of oil droplets or oil-soluble substances in water. Due to the design for stability in water, the structures of surfactants generally lack chemical bonds susceptible to oxidation–reduction reactions. Furthermore, based on the literature, the electrochemical oxidation of toluene often involves two main pathways [64–66]: 1. Direct electrooxidation using metal oxide electrodes and 2. generation of free radicals for indirect toluene oxidation. However, these methods cannot fully eradicate organic pollutants, as oxidized substances such as benzaldehyde and benzoic acid remain in solution [64,67].

4. Conclusions

In this work, an original combination of electro-demulsification and adsorption was applied to the treatment of O/W emulsions to decrease energy consumption. The crucial point of this technology is the special self-standing electrode. Carbonized birch biomass was chosen due to its naturally occurring, hierarchical, and orderly pore structure, high electrical conductivity, and strong mechanical properties. The distinctive porosity of wood allows it to accommodate substantial quantities of liquids and chemicals, offering exceptional capabilities for molecular diffusion and adsorption. Electrical force drove compression and collisions to promote demulsification in the limited pore space, and then small molecules in the pores were adsorbed by electrostatic force. The 5 % emulsion could be demulsified in 3.4 h at 5.0 V, and the removal

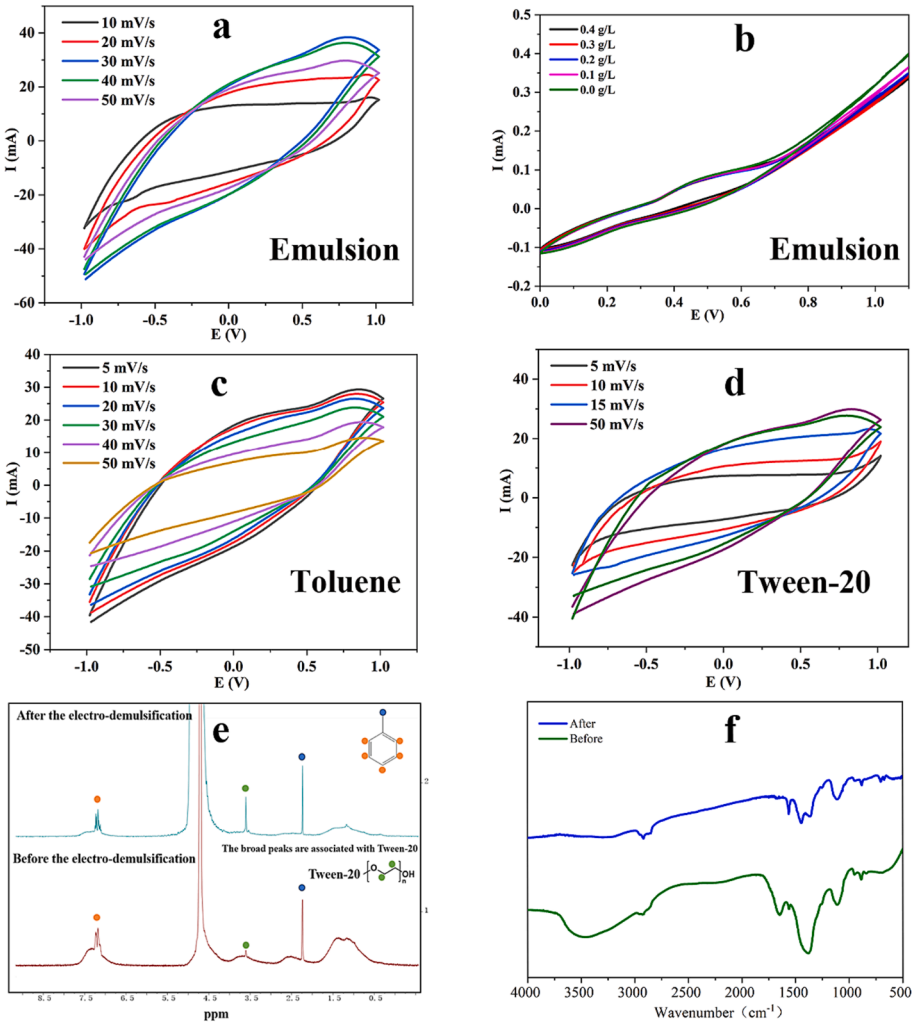

Fig. 12. (a) CV curves of a 1 % emulsion with different scan speeds (Tween-20 is 0.50 g/L). (b) CV curves of 1 % emulsions stabilized with different concentrations of Tween-20. (c) CV curves of saturated toluene solution at different scan speeds. (d) CV curves of Tween-20 solution (0.05 g/L) at different scan speeds. (e) Nuclear Magnetic Resonance characterization of emulsion samples before and after demulsification (The ^{1}H NMR peaks of O/W (Toluene and Tween-20) in D_2O). (f) Infrared spectroscopy analysis of emulsion samples before and after demulsification.

efficiency of toluene reached 97.97 %, with an electroadsorption capacity of 1180 mg g^{-1} and a power consumption level of 1.19 × 10^{-5} kWh. Solar as an energy source can be developed in the future to achieve convenience and environmental friendliness. This demulsification technology could realize demulsification with a low energy consumption level and remove organic pollutants in wastewater to a certain extent. This demulsification technology is worth popularizing.

CRediT authorship contribution statement

Kui Wang: Writing – review & editing, Writing – original draft, Investigation, Funding acquisition, Formal analysis, Data curation. **Hailiang Zhao:** Writing – review & editing, Software, Funding acquisition. **Yingming Zhang:** . **Xu Li:** Investigation. **Mengyi Xu:** Investigation. **Meirong Song:** . **Guangxin Ru:** . **Xiaolei Jiang:** . **Xiuhong Zhu:** . **Dandan Han:** . **Yutao Dong:** . **Kexin Shen:** . **Xinchang Pang:** . **Yuanyuan Li:** . **Yixiang Zhang:** Funding acquisition, Resources, Supervision. **Xia Sheng** supervised the project and contributed to the revision and discussion of the paper.

Declaration of competing interest

The authors declare that they have no known competing financial interests or personal relationships that could have appeared to influence the work reported in this paper.

Data availability

Data will be made available on request.

Acknowledgments

Financial support for this work was provided by the Key Science and Technology Program of Henan Province [grant numbers 202102210056 and 222102320428]; the Student's Platform for Innovation and Entrepreneurship Training Program of Henan Province [grant number 201910463050]; the Top-Notch Personnel Fund of Henan Agricultural University [grant number 30501033]; the Cultivation Program for Young Backbone Teachers in Henan University of Technology under the Natural Science Innovation Fund of Henan University of Technology [grant number 2020ZKCJ30]; the Fund of Longzihu New Energy Laboratory [grant number LZGLH2023011]; and the Fund of Public Group

Innovative Postdoctoral Practice Base, Corporate Postdoctoral [grant number ZZPU-PD-2023002]. We are grateful for the support from Wallenberg Wood Science Center [WWSC 2.0: KAW 2018.0452].

Appendix A. Supplementary data

Supplementary data to this article can be found online at https://doi.org/10.1016/j.cej.2024.148655.

References

[1] P. Chen, D. Yin, P.F. Song, Y.Y. Liu, L.K. Cai, H.L. Wang, L.H. Zhang, Demulsification and oil recovery from oil-in-water cutting fluid wastewater using electrochemical micromembrane technology, J. Clean. Prod. 244 (2020) 118698, https://doi.org/10.1016/j.jclepro.2019.118698.

[2] N.P. Aditya, S. Aditya, H.J. Yang, H.W. Kim, S.O. Park, S.H. Ko, Co-delivery of hydrophobic curcumin and hydrophilic catechin by a water-in-oil-in-water double emulsion, Food Chem. 173 (2015) 7–13, https://doi.org/10.1016/j.foodchem.2014.09.131.

[3] Z.N. Pintarič, G.P. Škof, Z. Kravanja, MILP synthesis of separation processes for waste oil-in-water emulsions treatment, Front. Chem. Sci. Eng. 10 (2016) 120–130, https://doi.org/10.1007/s11705-016-1559-1.

[4] H. Liang, H. Esmaeili, Application of nanomaterials for demulsification of oily wastewater: a review study, Environ. Technol. Innov. 22 (2021) 101498, https://doi.org/10.1016/j.eti.2021.101498.

[5] K. Guo, H.L. Li, Z.X. Yu, In-situ heavy and extra-heavy oil recovery: a review, Fuel. 185 (2016) 886–902, https://doi.org/10.1016/j.fuel.2016.08.047.

[6] F.J. Zhao, Z.X. Tian, Z.Q. Yu, H.Z. Shang, Y.P. Wu, Y.F. Zhang, Research status and analysis of stabilization mechanisms and demulsification methods of heavy oil emulsions, Energy Sci. Eng. 8 (2020) 4158–4177, https://doi.org/10.1002/ese3.814.

[7] K.L. Njoku, F.O. Okporuanefe, E.O. Ude, Responses of accessions of zea mays to crude oil pollution using growth indices and enzyme activities as markers, Pollution 4 (2018) 183–193, https://doi.org/10.22059/poll.2017.240286.306.

[8] S. Putatunda, S. Bhattacharya, D. Sen, S. Bhattacharjee, A review on the application of different treatment processes for emulsified oily wastewater, Int. J. Environ. Sci. Technol. 16 (2019) 2525–2536, https://doi.org/10.1007/s13762-018-2055-6.

[9] E.O. Bennett, Water based cutting fluids and human health, Tribol. Int. 16 (1983) 45–60, https://doi.org/10.1016/0301-679X(83)90055-5.

[10] Y.M. Shashidhara, S.R. Jayaram, Vegetable oils as a potential cutting fluid—An evolution, Tribol. Int. 43 (2010) 1073–1081, https://doi.org/10.1016/j.triboint.2009.12.065.

[11] J. Ma, X.G. Li, X.Y. Zhang, H. Sui, L. He, S.Y. Wang, A novel oxygen-containing demulsifier for efficient breaking of water-in-oil emulsions, Chem. Eng. J. 385 (2020) 123826, https://doi.org/10.1016/j.cej.2019.123826.

[12] Z.L. Zhang, G.S. Ai, G.X. Zeng, H.K. Yuan, Y. Yang, L.W. Shen, X.N. Feng, F. Ye, Y. Z. Mi, Demulsification of water-in-crude oil emulsion driven by a three-branch structure demulsifier, J. Mol. Liq. 354 (2022) 118822, https://doi.org/10.1016/j.molliq.2022.118822.

[13] Q.H. Cai, Z.W. Zhu, B. Chen, B.Y. Zhang, Oil-in-water emulsion breaking marine bacteria for demulsifying oily wastewater, Water Res. 149 (2019) 292–301, https://doi.org/10.1016/j.watres.2018.11.023.

[14] S.W. Fang, T. Chen, B. Chen, Y. Xiong, Y. Zhu, M. Duan, Graphene oxide at oil-water interfaces: Adsorption, assembly and demulsifification, Colloids Surf. A Physicochem. Eng. Aspects. 511 (2016) 47–54, https://doi.org/10.1016/j.colsurfa. 2016.09.058.

[15] X.P. Wang, W. Liu, X.Q. Liu, J.H. Luo, Study on demulsifification and deoiling for O/W emulsion by microbubble pretreated resin, Water Sci. Technol. 81 (2020) 148–158, https://doi.org/10.2166/wst.2020.095.

[16] J.S. Eow, M. Ghadiri, Electrostatic enhancement of coalescence of water droplets in oil, Chem. Eng. J. 85 (2002) 357–368, https://doi.org/10.1016/s1385-8947(01)00250-9.

[17] W.T. Kwon, K. Park, S.D. Han, S.M. Yoon, J.Y. Kim, W. Bae, Y.W. Rhee, Investigation of water separation from water-in-oil emulsion using electric field, J. Ind. Eng. Chem. 16 (2010) 684–687, https://doi.org/10.1016/j.jiec.2010.07.018.

[18] T. Ichikawa, K. Itoh, S. Yamamoto, M. Sumita, Rapid demulsification of dense oil-in-water emulsion by low external electric field: I. Experimental evidence, Colloids Surf. A Physicochem. Eng. Aspects. 242 (2004) 21–26, https://doi.org/10.1016/j.colsurfa.2004.04.053.

[19] T. Ichikawa, Y. Nakajima, Rapid demulsification of dense oil-in-water emulsion by low external electric field: II, Theory, Colloids Surf. A Physicochem. Eng. Aspects. 242 (2004) 27–37, https://doi.org/10.1016/j.colsurfa.2004.04.042.

[20] F. Shen, W. Luo, J.Q. Dai, Y.G. Yao, M.W. Zhu, E. Hitz, Y.F. Tang, Y.F. Chen, V. L. Sprenkle, X.L. Li, L.B. Hu, Ultra-thick, low-tortuosity, and mesoporous wood carbon anode for high-performance sodium-ion batteries, Chen. Adv. Energy Mater. 6 (2016) 1600377, https://doi.org/10.1002/aenm.201600377.

[21] F. Xin, Y.F. Jia, J. Sun, L.Q. Dang, Z.H. Liu, Z.B. Lei, Enhancing the capacitive performance of carbonized wood by growing FeOOH nanosheets and poly (3,4-ethylenedioxythiophene) coating, ACS Appl. Mater. Interfaces. 10 (2018) 32192–32200, https://doi.org/10.1021/acsami.8b11069.

[22] C. Jia, T. Li, C.J. Chen, J.Q. Dai, I.M. Kierzewski, J.W. Song, Y.J. Li, C.P. Yang, C. W. Wang, L.B. Hu, Scalable, anisotropic transparent paper directly from wood for light management in solar cells, Nano Energy. 36 (2017) 366–373, https://doi.org/10.1016/j.nanoen.2017.04.059.

[23] C. Chen, Y. Zhang, Y. Li, J. Dai, J. Song, Y. Yao, Y. Gong, L. Kierzewski, J. Xie, L. Hu, All-wood, low tortuosity, aqueous, biodegradable supercapacitors with ultra-high capacitance, Energy Environ. Sci. 10 (2017) 538–545, https://doi.org/10.1039/C6EE03716J.

[24] L. Elisadiki, T.E. Kibona, R.L. Machunda, M.W. Saleem, W.S. Kim, Y.A.C. Jande, Biomass-based carbon electrode materials for capacitive deionization: a review, Biomass Convers. Biorefin. 10 (2020) 1327–1356, https://doi.org/10.1007/s13399-019-00463-9.

[25] K.Z. Benis, J. Soltan, K.N. McPhedran, Electrochemically modified adsorbents for treatment of aqueous arsenic: Pore diffusion in modified biomass vs. biochar, Chem. Eng. J. 423 (2021) 130061, https://doi.org/10.1016/j.cej.2021.130061.

[26] X. Sheng, Y.Y. Li, T.M. Yang, B.J.J. Timmer, T. Willhammar, O. Cheung, L. Li, C. J. Brett, S.V. Roth, B.B. Zhang, L.Z. Fan, Y.X. Guo, X.D. Zou, L. Berglund, L.C. Sun, Hierarchical micro-reactor as electrodes for water splitting by metal rod tipped carbon nanocapsule self-assembly in carbonized wood, Appl. Catal. B Environ. 264 (2020) 118536, https://doi.org/10.1016/j.apcatb.2019.118536.

[27] C.Z. Zhu, S.F. Fu, J.H. Song, Q.R. Shi, D. Su, M.H. Engelhard, X.L. Li, D.D. Xiao, D. S. Li, L. Estevez, D. Du, Y.H. Lin, Self-assembled Fe-N-doped carbon nanotube aerogels with single-atom catalyst feature as high-efficiency oxygen reduction electrocatalysts, Small 13 (2017) 1603407, https://doi.org/10.1002/smll.201603407.

[28] H. Nishihara, Y. Fukura, K. Inde, K. Tsuji, M. Takeuchi, T. Kyotani, Carbon-coated mesoporous silica with hydrophobicity and electrical conductivity, Carbon 46 (2008) 48–53, https://doi.org/10.1016/j.carbon.2007.10.024.

[29] X. Sheng, N. Daems, B. Geboes, M. Kurttepeli, S. Bals, T. Breugelmans, A. Hubin, I. F.J. Vankelecom, P.P. Pescarmona, N-doped ordered mesoporous carbons prepared by a two-step nanocastin strategy as highly active and selective electrocatalysts for the reduction of O_2 to H_2O_2, Appl. Catal. B Environ. 176–177 (2015) 212–224, https://doi.org/10.1016/j.apcatb.2015.03.049.

[30] H. Esmaeili, F. Esmaeilzadeh, D. Mowla, Effect of surfactant on stability and size distribution of Gas condensate droplets in water, J. Chem. Eng. Data. 59 (2014) 1461–1467, https://doi.org/10.1021/je4009574.

[31] G. Güven, A. Perendeci, K. Özdemirc, A. Tanyolac, Specific energy consumption in electrochemical treatment of food industry wastewaters, J. Chem. Technol. Biotechnol. 87 (2012) 513–522, https://doi.org/10.1002/jctb.2739.

[32] J.J. Wei, X.P. Zhu, J.R. Ni, Electrochemical oxidation of phenol at boron-doped diamond electrode in pulse current mode, Electrochim. Acta. 56 (2011) 5310–5315, https://doi.org/10.1016/j.electacta.2011.04.006.

[33] N.D. Mu' azu, M. Al-Yahya, A.M. Al-Haj-Ali, I.M. Abdel-Magid, Specific energy consumption reduction during pulsed electrochemical oxidation of phenol using graphite electrodes, J. Environ. Chem. Eng. 4 (2016) 2477–2486, https://doi.org/10.1016/j.jece.2016.04.026.

[34] B. Saha, P.K. Bhattacharyya, Adsorption of amino acids on boron and/or nitrogen doped functionalized graphene: a density functional study, Comput, Theor. Chem. 1086 (2016) 45–51, https://doi.org/10.1016/j.comptc.2016.04.017.

[35] L. Sellaoui, T. Depci, A.R. Kul, S. Knani, A.B. Lamine, A new statistical physics model to interpret the binary adsorption isotherms of lead and zinc on activated carbon, J. Mol. Liq. 214 (2016) 220–230, https://doi.org/10.1016/j.molliq.2015.12.080.

[36] L. Sellaoui, D.I. Mendoza-Castillo, H.E. Reynel-Avila, B.A. Avila-Camacho, L. L. Diaz-Munoz, H. Ghalla, A. Bonilla-Petriciolet, A.B. Lamine, Understanding the adsorption of Pb^{2+}, Hg^{2+} and Zn^{2+} from aqueous solution on a lignocellulosic biomass char using advanced statistical physics models and density functional theory simulations, Chem. Eng. J. 365 (2019) 305–316, https://doi.org/10.1016/j.cej.2019.02.052.

[37] S.M. Cheng, S.S. Tang, N.T. Tsona, L. Du, The influence of the position of the double bond and ring size on the stability of hydrogen bonded complexes, Sci. Rep. 7 (2017) 11310, https://doi.org/10.1038/s41598-017-11921-7.

[38] Q. Zhang, L. Du, Hydrogen bonding in the carboxylic acid–aldehyde complexes, Comput. Theor. Chem. 1078 (2016) 123–128, https://doi.org/10.1016/j.comptc.2016.01.007.

[39] S. Tang, L. Du, Effects of methylation in acceptors on the hydrogen bond complexes between 2,2,2-trifluoroethanol and cyclic ethers, Spectrochim. Acta. A Mol. Biomol Spectrosc. 217 (2019) 237–246, https://doi.org/10.1016/j.saa. 2019.03.088.

[40] S. Tang, N.T. Tsona, L. Du, Ring-size effects on the stability and spectral shifts of hydrogen bonded cyclic ethers complexes, Sci. Rep. 8 (2018) 1553, https://doi.org/10.1038/s41598-017-18191-3.

[41] X.T. Jiang, N.T. Tsona, S.S. Tang, L. Du, Hydrogen bond docking preference in furans: OH···π vs, OH···O, Spectrochim. Acta. A Mol. Biomol. Spectrosc. 191 (2018) 155–164, https://doi.org/10.1016/j.saa.2017.10.006.

[42] S.Y. Li, H.G. Kjaergaard, L. Du, Infrared spectroscopic probing of dimethylamine clusters in an Ar matrix, J. Environ. Sci. 40 (2016) 51–59, https://doi.org/10.1016/j.jes.2015.09.012.

[43] M.J. Frisch, G.W. Trucks, H. B. Schlegel, G.E. Scuseria, M.A. Robb, J.R. Cheeseman, G. Scalmani, V. Barone, B. Mennucci, G.A. Petersson, H. Nakatsuji, M. Caricato, X. Li, H.P. Hratchian, A.F. Izmaylov, J. Bloino, G. Zheng, J.L. Sonnenberg, M. Hada, M. Ehara, K. Toyota, R. Fukuda, J. Hasegawa, M. Ishida, T. Nakajima, Y. Honda, O. Kitao, H. Nakai, T. Vreven, J.A. Montgomery Jr., J.E. Peralta, F. Ogliaro, M.J. Bearpark, J. Heyd, E.N. Brothers, K.N. Kudin, V.N. Staroverov, R. Kobayashi, J. Normand, K. Raghavachari, A.P. Rendell, J.C. Burant, S.S. Iyengar, J. Tomasi, M. Cossi, N. Rega, N.J. Millam, M. Klene, J.E. Knox, J.B. Cross, V. Bakken, C. Adamo, J. Jaramillo, R. Gomperts, R. E. Stratmann, O. Yazyev, A.J. Austin, R. Cammi, C. Pomelli, J.W. Ochterski, R.L. Martin, K. Morokuma, V.G. Zakrzewski, G.A. Voth, P. Salvador, , J.J. Dannenberg, S. Dapprich, A.D. Daniels, Ö. Farkas, J.B. Foresman, J.

V. Ortiz, J. Cioslowski, D.J. Fox, Gaussian 09, Revision E.01. Gaussian, Inc: Wallingford, CT, USA, 2013.
[44] R.S. Madyal, J.S. Arora, DFT studies for the evaluation of amine functionalized polystyrene adsorbents for selective adsorption of carbon dioxide, RSC Adv. 4 (2014) 20323–20333, https://doi.org/10.1039/C4RA00444B.
[45] M. Yi, Z.G. Shen, X.J. Zhang, S.L. Ma, Achieving concentrated graphene dispersions in water/acetone mixtures by the strategy of tailoring Hansen solubility parameters, J. Phys. d: Appl. Phys. 46 (2013) 025301, https://doi.org/10.1088/0022-3727/46/2/025301.
[46] G.X. Li, J.H. Sun, W.P. Hou, S.D Jiang, Y. Huan, J.X. Geng, Three-dimensional porous carbon composites containing high sulfur nanoparticle content for high-performance lithium-sulfur batteries, Nat. Commun. 7 (2016) 10601, https://doi.org/10.1038/ncomms10601.
[47] H.P. Boehm, Surface oxides on carbon and their analysis: A critical assessment, Carbon. 40 (2002) 145–149, https://doi.org/10.1016/S0008-6223(01)00165-8.
[48] B. Cao, J.P. Yuan, D. Jiang, S. Wang, B. Barati, Y.M. Hu, C. Yuan, X. Gong, Q. Wang, Seaweed-derived biochar with multiple active sites as a heterogeneous catalyst for converting macroalgae into acid-free biooil containing abundant ester and sugar substances, Fuel. 285 (2021) 119164, https://doi.org/10.1016/j.fuel.2020.119164.
[49] M.J. Fan, C. Li, Y.F. Sun, L.J. Zhang, S. Zhang, X. Hu, In situ characterization of functional groups of biochar in pyrolysis of cellulose, Sci. Total Environ. 799 (2021) 149354, https://doi.org/10.1016/j.scitotenv.2021.149354.
[50] J.C.Huang, Y. Qiao, Z.Q. Wang, H.P. Liu, B. Wang, Y. Yu, Valorization of food waste via torrefaction: effect of food waste type on the characteristics of torrefaction products, Energy Fuels 34 (2020) 6041–6051, https://doi.org/10.1021/acs.energyfuels.0c00790.
[51] M.J. Fan, Y.W. Shao, C. Li, F.M.B. Kontchouo, W.D. Ren, S. Zhang, S. Wang, B. Li, X. Hu, Balanced anchoring sites and volatile matter in biochar render Ni/biochar with higher metal dispersion and superior activity in hydrogenation of vanillin, Fuel 357 (2024) 129923, https://doi.org/10.1016/j.fuel.2023.129923.
[52] Y.C. Chiang, C.C. Liang, C.P. Chung, Characterization of platinum nanoparticles deposited on functionalized graphene sheets, Materials 8 (2015) 6484–6497, https://doi.org/10.3390/ma8095318.
[53] A.P. Terzyk, G. Rychlicki, The influence of activated carbon surface chemical composition on the adsorption of acetaminophen (paracetamol) in vitro: The temperature dependence of adsorption at the neutral pH, Colloids Surf. A Physicochem. Eng. Aspects. 163 (2000) 135–150, https://doi.org/10.1016/S0927-7757(99)00298-8.
[54] F. Yue, Q. Zhang, L.G. Xu, Y.Q. Zheng, C.X. Yao, J.N. Jia, W.N. Leng, S.F. Hou, Porous reduced graphene oxide/single-walled carbon nanotube film as freestanding and flexible electrode materials for electrosorption of organic dye, ACS Appl. Energy Mater. 2 (2019) 6258–6267, https://doi.org/10.3390/polym14152985.
[55] C. Janiak, A critical account on π–π stacking in metal complexes with aromatic nitrogen-containing ligands, J. Chem. Soc. Dalton Trans. 32 (2001) 3885–3896, https://doi.org/10.1002/chin.200111252.
[56] X.X. Zhou, L. Shi, T.B. Moghaddam, M.Z. Chen, S.P. Wu, X.Z. Yuan, Adsorption mechanism of polycyclic aromatic hydrocarbons using wood waste-derived biochar, J. Hazard. Mater. 425 (2022) 128003, https://doi.org/10.1016/j.jhazmat.2021.128003.
[57] R. Thakuria, N.K. Nath, B.K. Saha, The Nature and applications of π–π interactions: a perspective, Cryst. Growth Des. 19 (2019) 523–528, https://doi.org/10.1021/acs.cgd.8b01630.
[58] J.M. Lu, P.K. Mishra, T.N. Hunter, F. Yang, Z.G. Lu, D. Harbottle, Z.H. Xu, Functionalization of mesoporous carbons derived from pomelo peel as capacitive electrodes for preferential removal/recovery of copper and lead from contaminated water, Chem. Eng. J. 433 (2022) 134508, https://doi.org/10.1016/j.cej.2022.134508.
[59] E. Colleoni, G. Viciconte, C. Canciani, S. Saxena, P. Guida, W.L. Roberts, Sonoprocessing of oil: Asphaltene declustering behind fine ultrasonic emulsions, Ultrason. Sonochem. 98 (2023) 106476, https://doi.org/10.1016/j.ultsonch.2023.106476.
[60] S.S. Lee, M. Nakamura, Y. Takeuchi, Demulsification of o/w emulsion and subsequent water treatment using powder adsorbent, Korean J. Chem. Eng. 6 (1989) 81–87, https://doi.org/10.1007/bf02697483.
[61] G.Q. Xiao, Q.D. Meng, R.M. Wen, Adsorption of aspirin on the macropore resin with six functional group sites: Multiple functional group sites in macropore resin versus the micropore filling in hypercrosslinked resin, React. Funct. Polym. 151 (2020) 104581, https://doi.org/10.1016/j.reactfunctpolym.2020.104581.
[62] Y.L. Zhang, X.X.M.Y. Ran, Sorption of phenanthrene and benzene on differently structural kerogen: Important role of micropore-filling, Environ. Pollut. 185 (2014) 213–218, https://doi.org/10.1016/j.envpol.2013.10.039.39.
[63] M.N. Razali, A. Alhammadi, M. Musa, M.K. Nizam, A.E. Anuar, Comparison of natural adsorbent for emulsified wastewater treatment, IOP Conf. Ser. Mater. Sci. Eng. 1092 (2021) 012020, https://doi.org/10.1088/1757899X/1092/1/012020.
[64] A. Lindermeir, C. Horst, U. Hoffmann, Ultrasound assisted electrochemical oxidation of substituted toluenes, Ultrason. Sonochem. 10 (2013) 223–229, https://doi.org/10.1016/S1350-4177(03)00108-1.
[65] M. Michman, M. Oron, Oxidation of toluene linked with Ru(acac)3 catalysed electro-oxidation of water, Electrochim. Acta. 39 (1994) 1897–1901, https://doi.org/10.1016/0013-4686(94) 85182-4.
[66] L.F. D'Elia, L. Rincón, R. Ortíz,, Evaluation of titanium dioxide and cerium oxide as anodes for the electrooxidation of toluene: A theoretical approach of the electrode process, Electrochim. Acta. 49 (2004) 4197–4203, https://doi.org/10.1016/j.electacta.2004.04.014.
[67] S.E. Treimer, J. Feng, M.D. Scholten, D.C. Johnson, A.J. Davenport, Comparison of voltammetric responses of toluene and xylenes at Iron(III)-doped, bismuth(V)-doped, and undoped β-lead dioxide film electrodes in 0.50 M H_2SO_4, J. Electrochem. Soc. 148 (2001) E459, https://doi.org/10.1149/1.1413991.